MNRAS **000**, 000–000 (0000) Preprint 20 September 2016 Compiled using MNRAS LATEX style file v3.0

The disappearing act: A dusty wind eclipsing RW Aur

I. Bozhinova[1], A. Scholz[1], G. Costigan[2], O. Lux[3], C. J. Davis[4], T. Ray[5], N. F. Boardman[1], K. L. Hay[1], T. Hewlett[1], G. Hodosán[1], B. Morton[1]

[1]*SUPA, School of Physics and Astronomy, University of St Andrews, North Haugh, St Andrews, KY16 9SS, UK*
[2]*Leiden Observatory, University of Leiden, PB 9513, NL-2300 RA Leiden, the Netherlands*
[3]*Astrophysical Institute and University Observatory, Schillergässchen 2-3, 07745 Jena, Germany*
[4]*Liverpool John Moores University, Astrophysics Research Institute, Liverpool Science Park, IC2 Building 146 Brownlow Hill, Liverpool, L3 5RF, UK*
[5]*Dublin Institute for Advanced Studies, 31 Fitzwilliam Place, Dublin 2, Ireland*

arXiv:1609.05667v1 [astro-ph.SR] 19 Sep 2016

20 September 2016

ABSTRACT

RW Aur is a young binary star that experienced a deep dimming in 2010-11 in component A and a second even deeper dimming from summer 2014 to summer 2016. We present new unresolved multi-band photometry during the 2014-16 eclipse, new emission line spectroscopy before and during the dimming, archive infrared photometry between 2014-15, as well as an overview of literature data.

Spectral observations were carried out with the Fibre-fed RObotic Dual-beam Optical Spectrograph on the Liverpool Telescope. Photometric monitoring was done with the Las Cumbres Observatory Global Telescope Network and James Gregory Telescope. Our photometry shows that RW Aur dropped in brightness to R = 12.5 in March 2016. In addition to the long-term dimming trend, RW Aur is variable on time scales as short as hours. The short-term variation is most likely due to an unstable accretion flow. This, combined with the presence of accretion-related emission lines in the spectra suggest that accretion flows in the binary system are at least partially visible during the eclipse.

The equivalent width of [O I] increases by a factor of ten in 2014, coinciding with the dimming event, confirming previous reports. The blue-shifted part of the $H\alpha$ profile is suppressed during the eclipse. In combination with the increase in mid-infrared brightness during the eclipse reported in the literature and seen in WISE archival data, and constraints on the geometry of the disk around RW Aur A we arrive at the conclusion that the obscuring screen is part of a wind emanating from the inner disk.

Key words: Stars: variability – Stars: photometry– Stars: spectroscopy

1 INTRODUCTION

Classical T Tauri stars (TTS) are pre-main-sequence objects with strong irregular variability, first noted in a study of highly variable stars by Joy (1945). In that same work, RW Aur is identified as a T Tau type star with a spectrum rich in emission lines. Today, it is known that RW Aur is a visual binary with a separation of 1.4″ between the primary and secondary components. The spectrum of the primary shows strong signatures of accretion and winds (eg. Petrov et al. 2001; Alencar et al. 2005). The secondary, RW Aur B, is a late K type TTS (Ghez et al. 1993, 1997; White & Hillenbrand 2004) with little or no evidence of ongoing accretion. There are indications for the existence of more stellar/substellar companions in the system. The multiplicity study of T Tau stars by Ghez et al. (1993) reveals a possible tertiary component (RW Aur C) orbiting RW Aur B, with a separation of 0.12″ between the B and C stars. Furthermore, spectroscopic studies by Gahm et al. (1999) and Petrov et al. (2001) reveal periodic variations in the radial velocity of a number of lines in RW Aur A. The authors explore the possibility of a brown dwarf sized companion (RW Aur D) in close orbit around the primary as the cause for the observed spectroscopic variations.

Cabrit et al. (2006) examined CO maps of RW Aur from interferometry. They estimated the size of the circumstellar disk around RW Aur A to be unusually small (40-57 AU) and found evidence for a 600 AU long structure of material trailing from the primary star. The disk size was calculated for a disk inclination between 45-60°. Both the size of the disk and the "arm" were suggested as evidence for the tidal disruption of the circumstellar disk from a recent interaction with the secondary RW Aur B. This tidal interaction hyphothesis is further backed up by recent hydrodynamical simulations of the RW Aur disk by Dai et al. (2015).

In 2010 RW Aur underwent a long lasting dimming event,

© 0000 The Authors

that had never been observed before. The star dropped by ∼2 mag in the optical and remained in that state for several months. Rodriguez et al. (2013) presented a photometric investigation of this event, looking at KELT and American Association of Variable Star Observers (AAVSO) data. They conclude that the most likely explanation of this event is obscuration by material located ∼180 AU from RW Aur A. It is noted that the estimated occulting body lies far beyond the outer edge of the disk, but is still within the size of the tidally disrupted arm and therefore likely a part of it.

In 2014 RW Aur entered a second long lasting, even deeper (∼3 mag, Antipin et al. (2015)) minimum. Figure 1 shows an AAVSO visual lightcurve of RW Aur up until August 2016, including both dimming events. As can be seen in this lightcurve, there are clear signs that the star has recovered to its out-of-eclipse brightness in August 2016, indicating the end of the second eclipse. Our own photometry on Aug 25 and 26 confirms this, with R-band magnitudes of 10.7 and 10.6 (Scholz et al. 2016).

Petrov et al. (2015) performed a spectroscopic analysis of emission lines associated with accretion, wind and jets in and out of the 2014 minimum. They found enhancement in the equivalent widths of [O I] and [S II] (forbidden lines associated with jets), but no increase in the fluxes. Additionally, an increase in the strength of the resonant lines Ca II and Na I was reported. Furthermore, they found no change in the emission of Hα and He I, lines associated with accretion activity. The authors concluded that the obscuring body only covers the star and inner regions of the system, while the outer parts of the wind and jets remained unaffected. This effect was attributed to dust grains being lifted up into the line of sight through interactions with the winds. In addition, Shenavrin et al. (2015) report results of infrared photometry in JHKML in the period 2010-2015. They find a drop in JHK brightness corresponding to the 2014 dimming event, but a simultaneous increase in brightness in M and L. The excess IR emission is attributed to hot dust of about 1000 K, located around the inner disk rim, 0.1-0.2 AU away from the star. It is further speculated that the hot dust could then be lifted up into the wind, supporting the scenario presented in Petrov et al. (2015).

The dusty wind idea is in contrast to the tidal arm dimming scenario (Rodriguez et al. 2013, 2016) where an occultation by the tidal arm is expected to at least partially obscure the inner disk and possibly cover the excess IR emission. Rodriguez et al. (2016) also report a smaller dimming in 2012-13 and argue that the kinematics of this event fit the values derived from their analysis of the 2010 eclipse. Their analysis of the 2014 dimming using the same method is hampered by the fact that the ingress for the eclipse happened during the seasonal observing gap and its duration is not constrained yet. The tidal arm dimming scenario is potentially supported by the hydrodynamical simulations by Dai et al. (2015). Their simulations suggest the presence of material in a bridge between RW Aur A and B, with several particles also crossing the line-of-sight to the system.

Finally, Takami et al. (2016) present a spectroscopic study of the system between Oct 2010 and Jan 2015 and argue that neither the tidal arm nor dusty wind scenario alone can account for the complex variability seen in the lines in and out of the eclipses. The authors further explore time-variable mass accretion as an alternative explanation to the observed dim and bright states of the system within the 2010-15 time frame.

In this study we present photometric and spectroscopic observations of RW Aur taken just before and during the 2014 dimming. We explore the photometric variability in several optical and infrared bands along with equivalent width and profile analysis of the Hα, He I and [O I] lines to provide further evidence to the above scenarios.

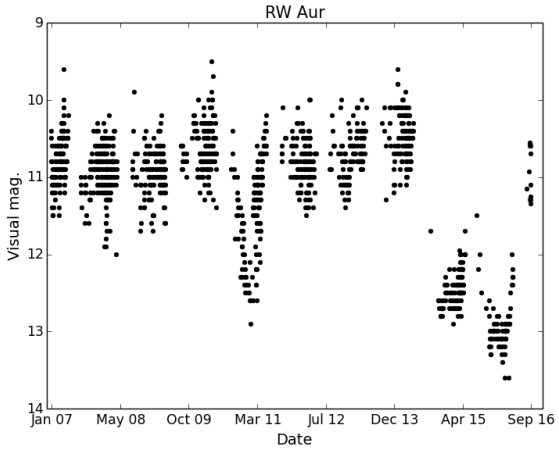

Figure 1. American Association of Variable Star Observers (AAVSO) visual lightcurve for RW Aur between 2007 and 2016. The 2010 and 2014 dimmings are clearly visible.

2 OBSERVATIONS AND DATA REDUCTION

2.1 LCOGT

A portion of the photometric data presented in this work was taken with the Las Cumbres Observatory Global Telescope Network (LCOGT) (Brown et al. 2013) as part of programs STA2014B-002 and STA2015A-002. This set spans the period 26 Dec 2014 - 11 Jan 2016. All images were taken with SBIG cameras on 1-meter telescopes. The detectors have a size of 4K × 4K pixels, 9 μm pixel size, field of view of $15.8 \times 15.8'$ and resolution of $0''.464$/pix. Each epoch consist of a set of images of 10s and 100s exposure time in four bandpasses (Sloan u', g', r' and i', Fukugita et al. 1996). In some cases, where observations have been interrupted and resumed, we have multiple images per epoch. The main science frames are the 100s exposures, the shorter exposures were taken in the event of saturation of objects in the field, but have not been used in the current work. Table 1 summarises the epochs and exposures for each filter. The raw images have been reduced with the LCOGT data reduction pipeline[1].

2.2 JGT

As a complement to the LCOGT observations, we have also monitored RW Aur with the 0.94-meter James Gregory Telescope (JGT) at the University of St Andrews Observatory. The JGT has an Andor CCD detector, 1K × 1K pixels, 13μm pixel size, resolution of $\sim 1''.0$/pix and a field of view of about $15' \times 15'$. At each epoch we continuously monitored the target for a period of at least 1 hour in the Cousin R-band in order to explore its short time-scale behaviour. The exposure time is 30-60 s, depending on conditions. The JGT dataset (summarised in Table 2) was taken between March

[1] http://lcogt.net/observatory/data/pipeline/

Table 1. Summary of epochs and number of 100s exposures per epoch in each filter from the LCOGT data set.

MJD	Date	u′ (3543 Å)	g′ (4770 Å)	r′ (6231 Å)	i′ (7625 Å)
57017	26-12-2014	0	3	3	3
57020	29-12-2014	1	2	2	2
57038	16-01-2015	1	1	1	1
57041	19-01-2015	1	1	1	2
57043	21-01-2015	1	1	1	1
57046	24-01-2015	1	1	1	1
57049	27-01-2015	1	2	2	2
57051	29-01-2015	1	3	2	2
57056	03-02-2015	1	1	1	1
57058	05-02-2015	1	1	1	1
57062	09-02-2015	0	2	2	2
57077	24-02-2015	1	1	1	1
57088	07-03-2015	1	1	1	1
57092	11-03-2015	1	1	1	2
57097	16-03-2015	1	0	1	1
57104	23-03-2015	1	1	1	1
57109	28-03-2015	0	1	1	1
57258	24-08-2015	1	1	1	1
57260	26-08-2015	1	1	1	1
57262	28-08-2015	1	1	1	1
57264	30-08-2015	1	1	1	1
57266	01-09-2015	1	1	1	1
57268	03-09-2015	1	1	1	1
57270	05-09-2015	1	1	1	1
57278	13-09-2015	1	1	1	1
57280	15-09-2015	1	1	1	1
57292	27-09-2015	1	1	1	1
57294	29-09-2015	1	1	1	1
57315	20-10-2015	1	1	1	1
57321	26-10-2015	1	1	1	1
57323	28-10-2015	2	2	2	1
57352	26-11-2015	1	1	1	1
57360	04-12-2015	1	1	1	1
57365	09-12-2015	1	1	1	1
57367	11-12-2015	1	1	1	1
57372	16-12-2015	1	1	1	1
57375	19-12-2015	1	1	1	1
57377	21-12-2015	1	1	1	1
57380	24-12-2015	1	1	1	1
57382	26-12-2015	1	1	1	1
57395	08-01-2016	1	1	1	1
57398	11-01-2016	1	1	1	1

2015 and March 2016. Standard reduction including bias subtraction and flat-fielding was performed.

2.3 Spectral observations

Spectral observations were performed with FRODOSpec (Fibre-fed RObotic Dual-beam Optical Spectrograph), a robotic integral field spectrograph on the Liverpool Telescope (Steele et al. 2004). Data covers 19 nights between February 2013 and February 2015 with three spectra taken each night (Table 3). Both blue (3900 - 5100Å) and red arm (5900 - 8000 Å) observations were completed. Due to the very low S/N, the blue arm spectra were not considered in the following work. The resolution of the red arm in high resolution mode is ∼ 5,300. The integral field covers 9.″84× 9.″84, with 12 lenslets each with diameter of 0.″82 on-sky. The exposure time is 300s for all spectra.

Table 2. Summary of photometric observations with the JGT. This table lists date, number of images, exposure time and average Cousin R-band magnitude of RW Aur for each night.

MJD	Date	no images	t exp. (s)	R (mag)
57092	11-03-2015	270	60	11.89
57099	18-03-2015	160	60	12.21
57104	23-03-2015	110	60	11.99
57110	29-03-2015	130	60	12.08
57337	11-11-2015	240	30	12.71
57367	11-12-2015	210	60	12.47
57368	12-12-2015	270	30	12.53
57401	14-01-2016	250	60	12.54
57428	10-02-2016	320	60	12.65
57429	11-02-2016	240	60	12.61
57454	07-03-2016	240	30	12.41
57478	31-03-2016	110	60	12.43

Due to the robotic nature of the telescope, in some of the observations the source is either not within the integral field unit (IFU) or is not centred within the IFU. The main result appears to be an increase in the noise within the spectrum. We only considered the cases where the PSF peak lies within the IFU. In the majority of cases the full PSF lies completely within the IFU. In some cases (see Table 3), the peak of the PSF lies on the edge of the detector (as noted by the spread in the PSF across the IFU edge), and so we are missing flux from one of the wings of the PSF. We tested for differences in the measured EW in these epochs and no significant difference was seen.

We reduce the data using the FRODOSpec pipeline (Barnsley et al. 2012). The pipeline first performs basic CCD processing, including bias subtraction, overscan trimming and CCD flat fielding. A continuum lamp is used to find the fibre positions and find a polynomial trace for each. Flux is extracted for each fibre in the target frame, continuum and arc lamp frames. Wavelength calibration is then performed for each spectrum and transmission correction, using the continuum lamp. The spectra are rebinned in order to determine a single wavelength solution for the entire data cube. Finally, sky extraction is done by combining the signal from sky only fibers. The spectra are not flux calibrated. We also do not resolve RW Aur A and B.

3 DATA ANALYSIS

3.1 Photometry

For the LCOGT and JGT images we perform aperture photometry using the standard photometric IRAF package *daophot*[2]. We measure RW Aur along with 10-15 well exposed, unsaturated comparison stars. The aperture is set to 2.5 times the FWHM of the PSF. We construct differential lightcurves by calculating a reference lightcurve from well-exposed comparison stars and subtracting that from the RW Aur raw lightcurve. This ensures systematic effects such as variable weather conditions are removed from the final data. The reference curves were inspected for any outlying points and a few epochs were removed (due to proximity of the Moon).

The lightcurves derived from the LCOGT data are presented

[2] http://iraf.noao.edu/docs/photom.html

Table 3. Summary of spectral observation epochs and mean equivalent width measurements for the Hα, [O I] and He I emission Line. All EWs are in Å. Epochs in which the target was not centred in the IFU i.e. not completely covered, are indicated in the last column.

MJD	Date	H α	[O I]	He I	IFU coverage
56330	07-02-2013	83.88	0.54	1.01	Partial
56363	12-13-2013	88.07	0.54	0.37	Complete
56500	27-07-2013	77.94	0.7	0.42	Complete
56524	20-08-2013	74.87	0.62	1.09	Complete
56544	09-09-2013	55.39	0.37	0.6	Complete
56565	30-09-2013	35.53	0.36	0.49	Complete
56586	21-10-2013	60.79	0.55	0.64	Complete
56611	15-11-2013	78.96	0.49	0.64	Complete
56644	18-12-2013	42.68	0.69	1.11	Complete
56671	14-01-2014	51.9	0.61	0.65	Complete
56724	08-03-2014	52.21	0.48	0.35	Complete
56740	24-03-2014	45.39	0.55	0.43	Complete
56752	05-04-2014	69.7	0.54	1.13	Complete
56910	10-09-2014	21.29	1.9	0.5	Partial
57028	06-01-2015	17.97	2.61	0.4	Partial
57034	12-01-2015	16.05	4.63	0.14	Complete
57039	17-01-2015	32.25	4.96	0.32	Partial
57049	27-01-2015	26.59	5.75	0.18	Partial
57079	26-02-2015	23.81	3.64	0.72	Partial

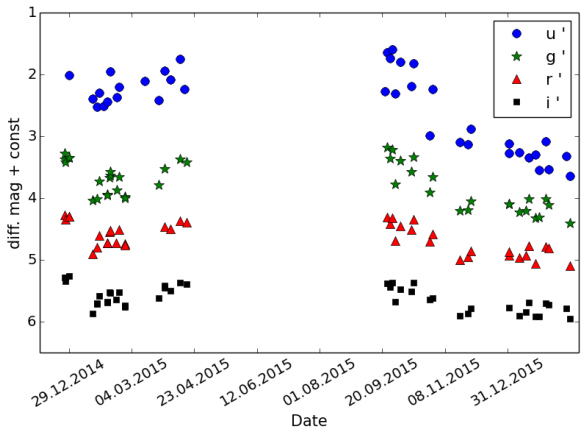

Figure 2. RW Aur lightcurves from LCOGT data. *Blue circles* - u′ band (3543 Å), *green stars* - g′ band (4770 Å), *red triangles* - r′ band (6231 Å), *black squares* - i′ band (7625 Å). The lightcurves are shifted by an arbitrary constant for clarity. All lightcurves show a similar shape.

in Figure 2. Photometric accuracy (defined as the lower envelope of the RMS of the reference stars) is on the order of a few percent, with RW Aur being a clear, highly variable outlier. The RW Aur curves in the four bands have similar shapes and amplitudes (between 0.7-2.1 mag, Table 4). The amplitudes are calculated as the max-min difference with an uncertainty of about 0.02 mag. A visual inspection shows a very good correlation between the shape of the lightcurves in the r′and i′-bands, but the correlation becomes weaker towards the bluer wavelengths. The brightness of RW Aur has continued to decline throughout the 2015-2016 winter observing season in all filters. The similarity in the shapes of the lightcurves in the separate bands before and after the 2015 observing gap suggests the continued drop in flux is caused by the same source as the initial eclipse in 2014.

Table 4. Amplitudes (A) and reddening slopes for the observed data and interstellar extinction. The error for the observed amplitudes is 0.02 mag. The observed slopes correspond to the best (linear regression) fit to the photometric data. We use the extinction law by Cardelli et al. 1989 to calculate extinction amplitudes and reddening slopes. In this table, we present the amplitudes and slopes calculated for $R_V = 3.1$ and $A_V = 0.9$, which are the parameter values producing the best fit to the observed r-band amplitude.

Bands	**Obs. A**	**Exct. A**
u	2.05	1.49
g	1.22	1.12
r	0.81	0.81
i	0.70	0.61
Color	**Obs. slope**	**Exct. slope**
u-g	1.82	4.08
g-r	2.8	3.68
r-i	3.89	4.02

Standard aperture photometry was applied to the JGT images using ∼6 reference stars. The R-band was shifted to standard using the USNO-B1.0 magnitudes for 3 reference stars (Monet et al. 2003). The error is ∼0.01 mag. The differential lightcurves are presented in Figure 3. The lightcurves show a significant irregular variability (up to 0.2 mag) on timescales of hours.

3.2 Mid-IR WISE archival data

In Figure. 4 we present archive post-cryo WISE (NEOWISE, Mainzer et al. 2011, 2014) observations of RW Aur between 2014 and 2015. This dataset consists of four blocks of observations, each consisting of several measurements over the course of 1-2 consecutive nights. The first block has been taken prior to the start of the 2014 dimming while the remaining three blocks are in the faint state. The red datapoints represent the average value of the measurements of a given block. The star shows clear variability on timescales of hours and days in all blocks. After the dimming, the average magnitude in W1 and W2 increases by 0.14−0.26 and 0.66−1.28 mag respectively. The photometric error is ∼0.03 mag in W1 and ∼0.01 mag in W2. The changes in the average values in the WISE bands after the eclipse are comparable to the M and L-band brightenings reported by Shenavrin et al. (2015), therefore solidifying the evidence for the mid-IR excess emission increase coinciding with the dimming in the optical.

3.3 Spectral analysis

The FRODOSpec spectra show clear emission lines typically associated with accretion (Hα (6563 Å) and He I (6678 Å)) and outflow ([O I] (6300 Å)). We present profile timeseries for the Hα and [O I] lines in Figure 5 and 6. We measure equivalent widths (EWs) for these three lines. There are three measurements for each consecutive night. We normalize all spectra within the same spectral range to minimise any variability from changing weather conditions. The IFU positioning does not seem to have an effect on EWs. The results are presented in Figure 7, 8 and Table 3. The errors in the plots are taken to be the spread in measurements over one night (3 observations). We observe a drop in Hα and increase in the [O I] during the dimming event. The He I shows no significant change. The Hα EW drops from 80−90 Å in the bright state down to ∼20 Å in the dim state. However, we note the Hα EW begins to decrease prior

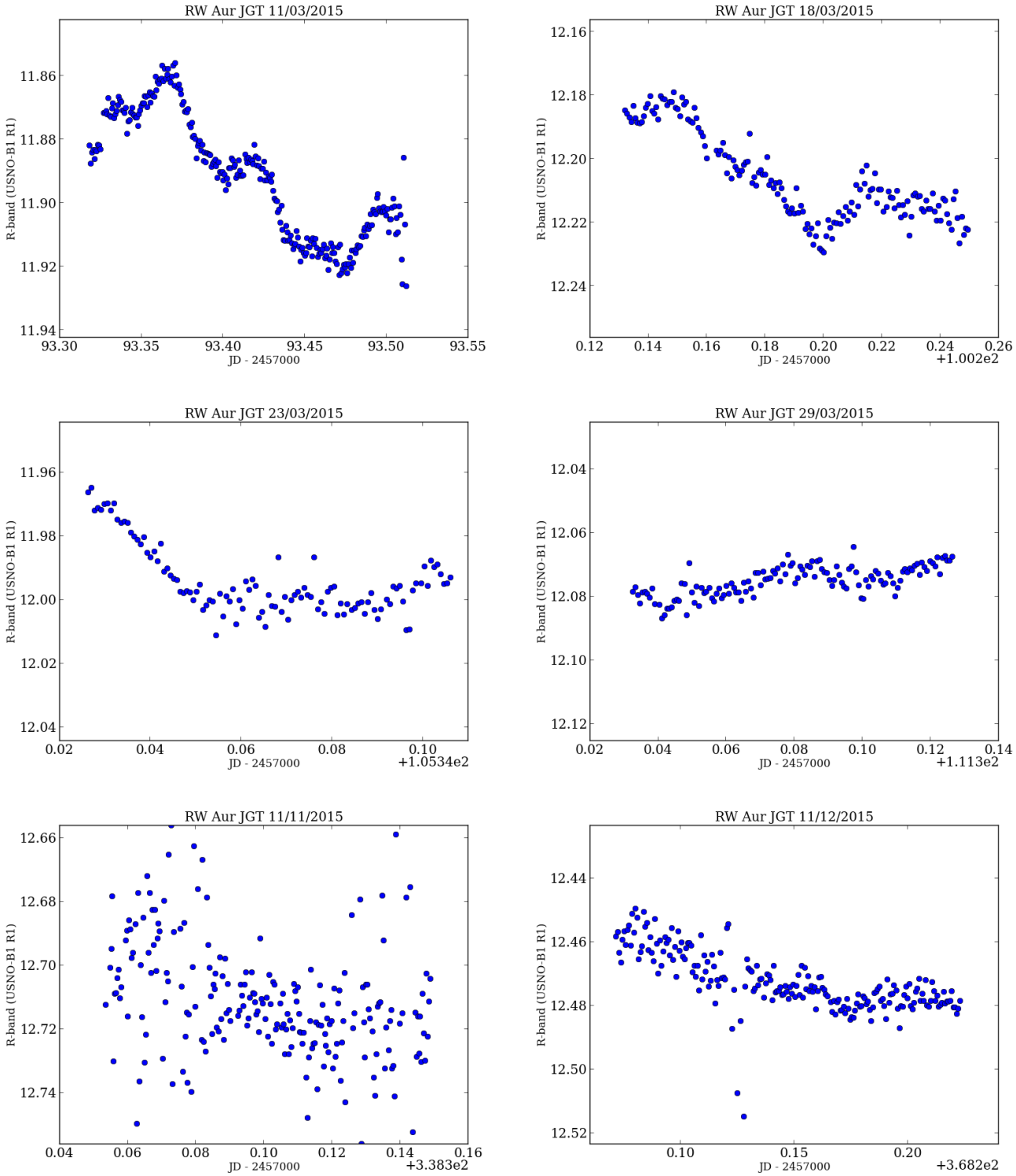

Figure 3. RW Aur JGT lightcurves, R-band. Significant irregular variability (up to 0.2 mag) on time-scales of hours can be seen throughout the entire observing season.

to the 2014 eclipse (Fig. 7) and it is therefore possible the change in Hα EW is not solely related to the dimming event, as the line is known to be intrinsically variable (Petrov et al. 2001; Alencar et al. 2005). The [O I] EW increases from 0.5 to 5 Å, i.e. by a factor of 10.

We also show timeseries of the Hα and [O I] profiles in Figure 5 and 6. In each case the date is given beside the mean profile for that night. The characteristic broad, double-peaked profile of the Hα line can clearly be seen in both the bright and dim state. However, during the dimming the entire profile is suppressed and the

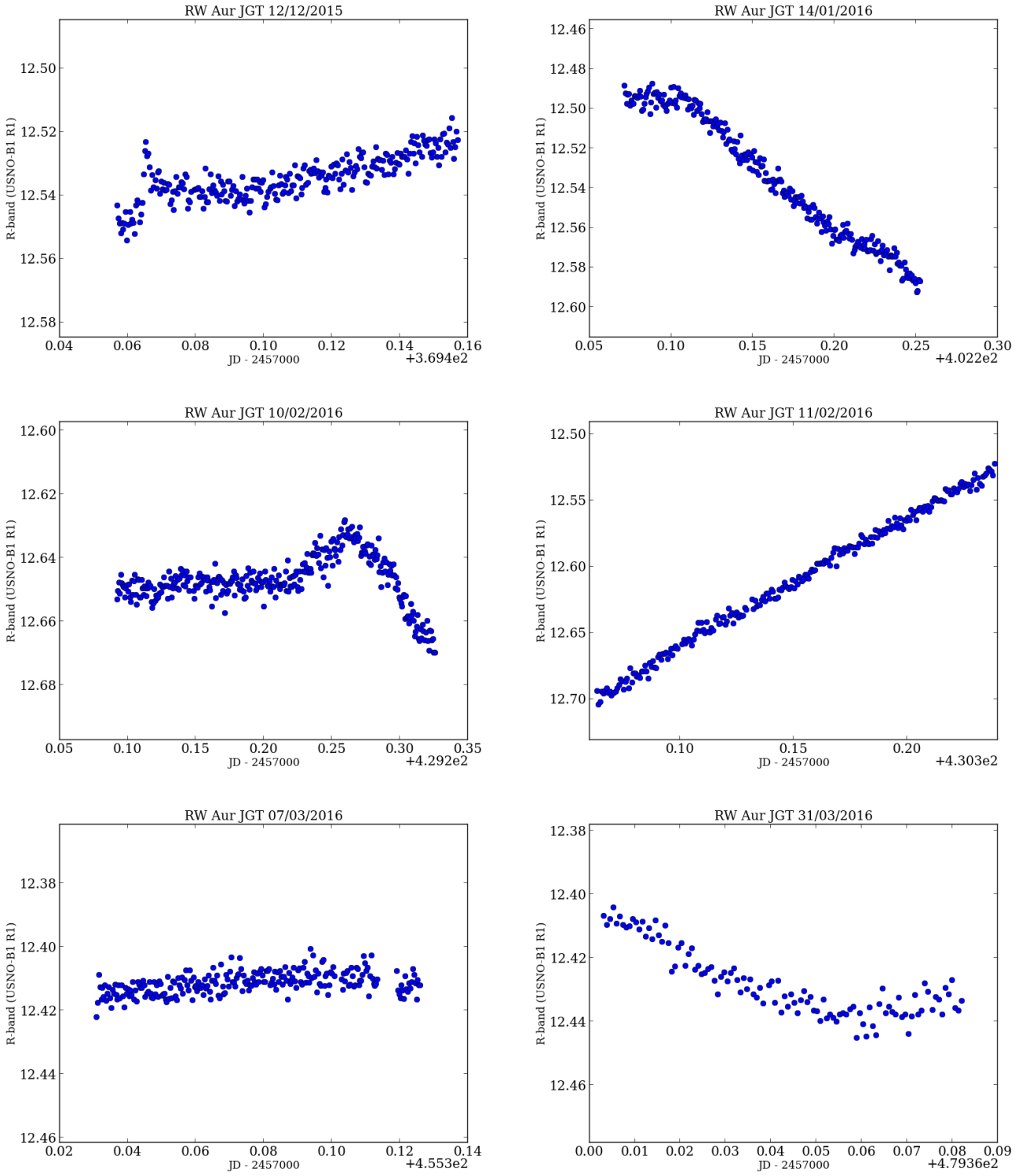

Figure 3 (continued).

blue-shifted peak appears significantly weaker than the red-shifted peak. We measure the Hα EW for v<0 km/s and v>0 km/s in order to quantify the difference between the change in the blue and red-shifted peaks after the dimming. The line EW decreases by a factor of ~7 after the eclipse for v<0 km/s and by a factor of ~3 for v>0 km/s. The difference in the two factors suggests that the blue-shifted peak suppression is indeed significant. In contrast to the Hα line, the [O I] profile becomes more prominent during the dimming, showing a broad and asymmetric emission.

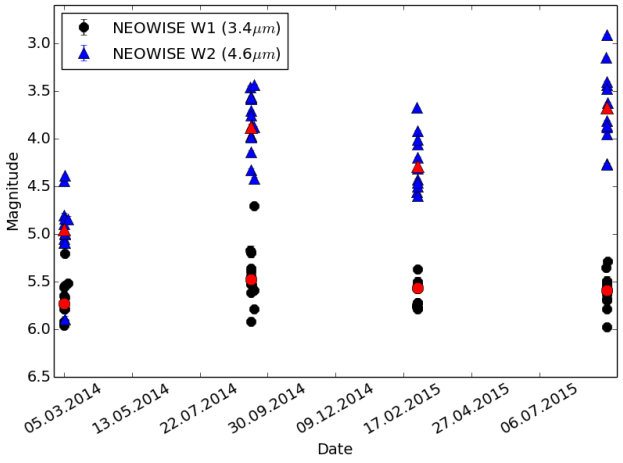

Figure 4. NEOWISE observations of RW Aur before and after the 2014 dimming. The red datapoints represent the average magnitude of RW Aur for each observational block. The system becomes brighter in both bands during the 2014 eclipse (see Sect 3.2).

4 DISCUSSION

We present new spectroscopic and photometric observations of RW Aur during the dimming in 2014-2016. In addition, we review the previous and new observational constraints for the system.

4.1 Photometric variations

The dimming event that started in 2014 is continuing through our observing period. The system has become even fainter in the optical during the 2015-16 winter observing season (see Figures 1 and 2). In addition to the long-term dimming trend, we clearly see irregular short timescale variations in the JGT (Figure 3) and LCOGT (Figure 2) data. These variations could be related to small scale changes in extinction along the line of sight. However, the irregular components in the morphology of the JGT lightcurves better resemble burst-like events. Such morphology is typically associated with changes in an unstable accretion flow for T Tau stars (see Herbst et al. 1994; Cody et al. 2014 for an overview of the different types of photometric variability displayed by T Tau stars). Being able to see such short time-scale irregular variations in RW Aur implies that the accretion flow in the system remains at least partially visible during the dimming.

In addition to the overall drop in photometric flux in the optical, colour-magnitude diagrams of our LCOGT data (Figure 9) reveal a significant long-term reddening trend since the start of the eclipse. We compare the observed reddening with models for interstellar extinction by Cardelli et al. (1989). Extinction fails to fit the observed colours simultaneously. In particular, the model underpredicts the observed u′-band amplitude and is unable to reproduce the u′ − g′ reddening slope. We therefore conclude that the long-term reddening trend is not consistent with interstellar-like extinction.

We also attempt to explain the reddening with a simple hot spot model, where the star and spots are approximated by black bodies and the spot temperature and filling factor are varied in order to fit the observed lightcurve amplitudes (eg. Scholz et al. 2009, Bouvier et al. 1995).

We find a number of parameter values that produce amplitudes and reddening slopes similar to the observed ones, especially in the red portion of the spectrum. However, hot spots have one major problem with explaining the observed long-term reddening. Hot spots form at the stellar surface as a result from accreting material near-free falling onto the star and creating shocks. As the star rotates the spots come in and out of view, resulting in a photometric variably on time-scales comparable with the stellar rotational period (typically several days for T Tau stars). This is in contrast to the long-term dimming of RW Aur which has lasted for months. While accretion may still play a role for the short-time scale variability of RW Aur, hot spots cannot be the cause for the observed

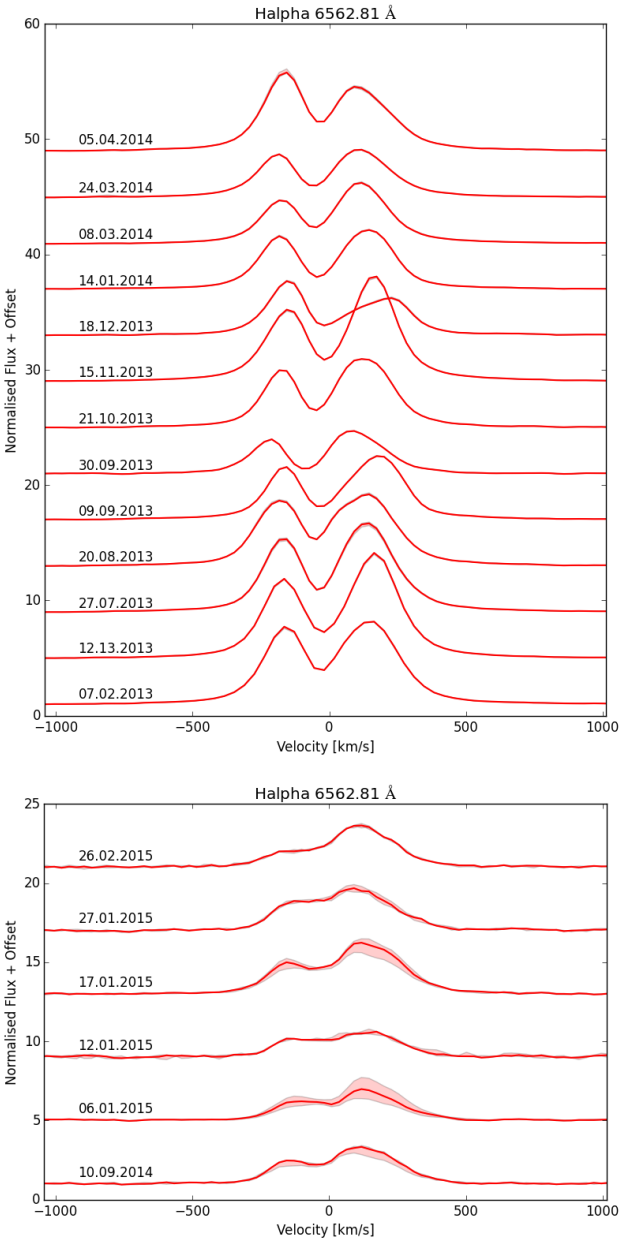

Figure 5. Full time-series of all Hα profiles. The top panel shows the observations before the dimming event and the bottom panel shows the spectra taken after the start of the eclipse. The red lines indicate the mean profile for that night's observation. The red shading indicates the spread between the individual 3 spectra for that night.

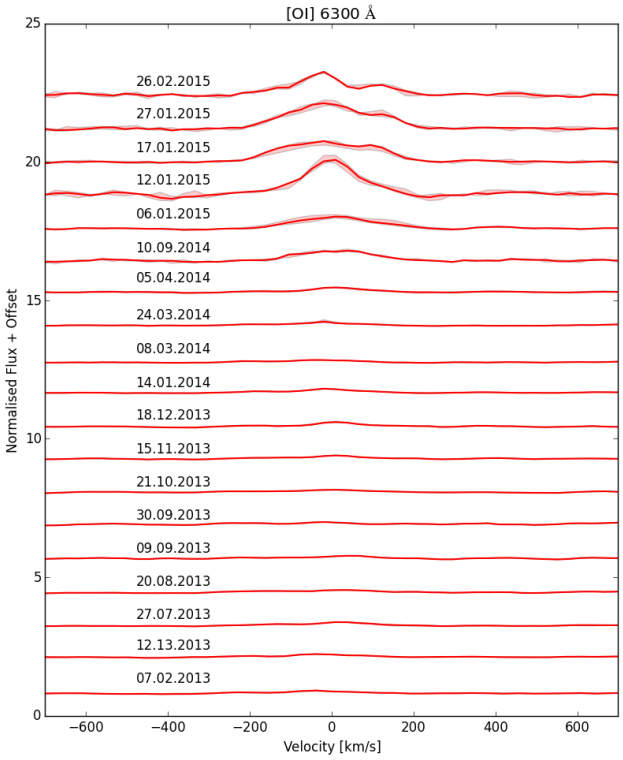

Figure 6. Partial time series of the [O I] profiles. The red lines indicate the mean profile for that night's observation. While the red shading indicates the spread between the individual 3 spectra for that night.

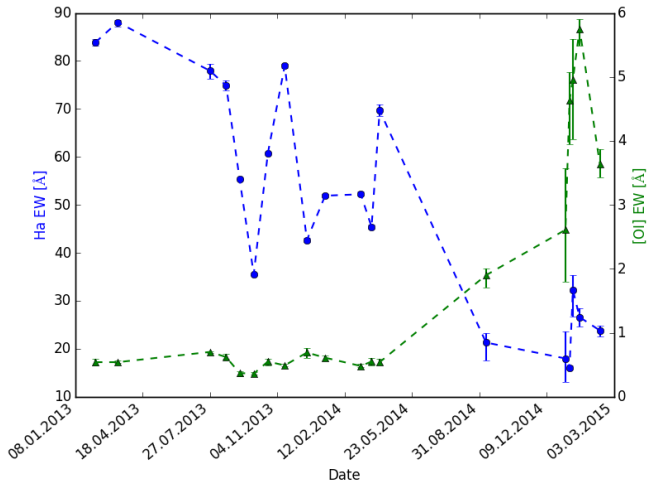

Figure 7. Mean EW versus date for Hα (blue dots) and [O I] (green triangles). Here the mean EW is taken from the 3 observations each night. The error bars represent the differences between the 3 observations that night. We see an increase in the [O I] by a factor of 10 after the dimming. We also observe a drop in the Hα EW.

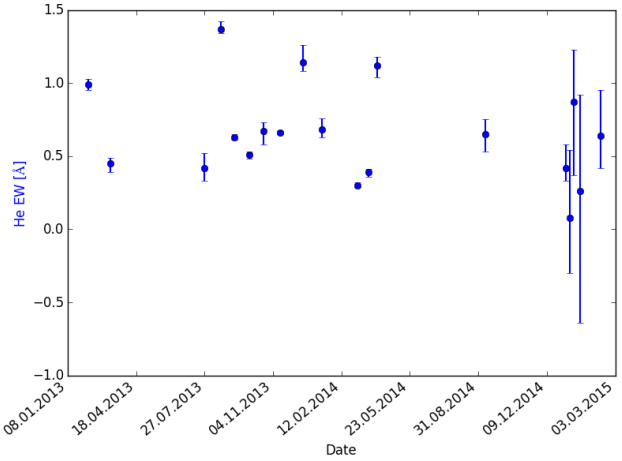

Figure 8. Mean EW versus date for He I. Here the mean EW is taken from the 3 observations each night. The error bars represent the differences between the 3 observations that night. No significant change in the He I EW is observed.

long-term reddening, where the system has continuously been getting redder for months.

An alternative explanation for the observed long-term reddening arises from the fact that our photometry does not resolve RW Aur A and B. Antipin et al. (2015) present resolved photometry of the system. Their measurements (after the start of the dimming) show an R-band magnitude of 13.08 and 11.97 for the A and B-components respectively. Our JGT photometry yields R~12 mag suggesting that the red part of the spectrum in our observations is most likely dominated by the B-component. We can therefore interpret the observed long-term reddening as the A-component becoming faint enough that the B-component becomes the dominant source of flux, making the entire system appear redder while simultaneously getting dimmer as we lose flux from RW Aur A.

4.2 Spectral signatures

Spectroscopy provides more information about accretion and outflow in young stellar systems. In the classical magnetospheric accretion scenario the inner-most region of the circumstellar disk is threaded by stellar magnetic field lines. Material is channelled from the disk onto the star forming accretion columns at near free-fall velocities, with a shock forming at the surface of the star. The shock and accretion columns generate Hα emission. The accretion-related Hα emission lines are typically broad with equivalent widths of over 10 Å. Other emission lines related to CTTS accretion include permitted lines of He I, O I and Ca II. For a review of accretion signatures we refer the reader to Mohanty et al. (2005) and references therein. In addition to accretion indicators, CTTS often shows outflow-related forbidden line emission such as [O I] lines (Hartigan et al. 1995; Appenzeller et al. 1984).

Our spectra show that the EW of the [O I] (6300 Å) line increases by a factor of 10 after the eclipse (Figure 6,7). The observed EW increase is in agreement with measurements by Petrov et al. (2015) and Takami et al. (2016). Petrov et al. (2015) attribute the change in the forbidden line's EW to a drop in the photospheric continuum, as reported by the resolved photometry of RW Aur A by Antipin et al. (2015). Petrov et al. (2015) further imply that the ob-

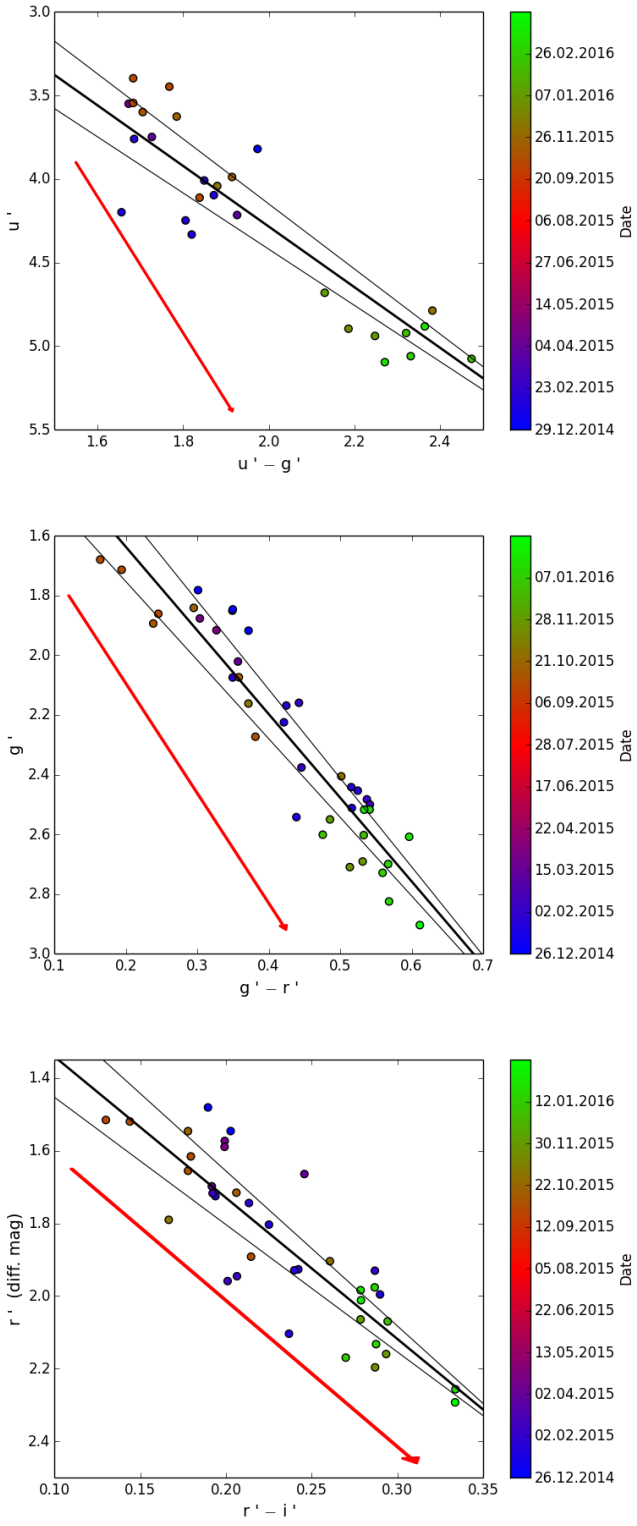

Figure 9. Colour-magnitude diagrams constructed from all LCOGT observations. The epochs of observations are colour coded. The black solid line indicates the best linear fit to the data with thinner lines indicating the error in the slope estimation. The red arrow is the interstellar extinction slope for $R_V = 3.1$ and $A_V = 0.9$, where the A_V value is selected such that the resulting extinction in the r-band best matches the observed amplitude in the r-band lightcurve.

scuring body must be blocking the inner parts of the system while the outflow remains visible.

The He I (6678 Å) and Hα emission lines remain clearly visible in our spectra after RW Aur enters the eclipse. This again indicates that at least part of the accretion flow is still visible. The He I EW remains constant (Figure 8), implying the He-emitting regions are obscured in the same way as the photosphere.

The Hα EW decreases after the eclipse (Figure 7). Our EW measurements show lower values for the line during the dimming compared to the values reported by both Petrov et al. (2015) and Takami et al. (2016). We attribute this to the fact that our spectroscopy does not resolve the A and B-components, hence we get an additional flux in the continuum from RW Aur B, resulting in a lower EW value.

The Hα line profiles show a suppressed blue-shifted peak after the start of the dimming (Figure 5). This can also be seen in the Hα profiles from Takami et al. (2016) from both the 2010 and 2014 dimmings. This blue-shifted absorption can be interpreted as the presence of an absorbing material moving towards the observer's line-of-sight, i.e. an outflow.

4.3 Origin of the eclipse

In Sect. 1 we introduce two possible explanations for the long dimming event observed in RW Aur. The obscuring screen could either be a tidal arm in the outer disk, as suggested by Rodriguez et al. (2013, 2016), or a wind emanating in the inner disk, suggested by Petrov et al. (2015). Our observations provide new evidence to support the occultation by a wind.

In particular, we show that the blue-shifted portion of the Hα line is suppressed since the beginning of the eclipse, indicating the presence of outflowing and thus blueshifted gas with velocities of 100-200 kms^{-1} in the occulting screen. This scenario is further supported by the increase in the mid-IR fluxes of the system in eclipse, reported by Shenavrin et al. (2015) and visible in archive NEOWISE data in the W2 band (Figure. 4). Shenavrin et al. (2015) fit a blackbody to the spectral energy distribution of RW Aur in its faint state and find that the excess IR emission is plausibly explained by the presence of hot dust with temperature around 1000 K along the line of sight.

Thus, the occulting body is outflowing and contains hot dust, which fits with a scenario where a wind emanating from the inner disk eclipses the star RW Aur A. These two facts together are also inconsistent with the tidal arm scenario, in which the occulting material would not be expected to move rapidly along the line of sight and the dust in the screen would be cold. If the eclipse indeed arises in a wind, the long duration of the current event would imply that the outflowing screen stretches azimuthally over a large portion of the inner disk. We note that the recent resolved X-ray detection of RW Aur shows a slight soft X-ray extension of RW Aur A along the blue-shifted jet axis close to the star (Skinner & Güdel 2014) - this could be related to the obscuring screen discussed here. Furthermore, Schneider et al. (2015) present resolved X-ray and NIR observations of the system in eclipse and provide further evidence for the presence of an obscuring screen with hot material located close to the star.

In addition, there is also a geometrical argument in favour of a blocking screen located above the inner disk. The CO map modelling from Cabrit et al. (2006) found an inclination between 45-60° for the large-scale disk. The inclination of the jet to the line of sight is measured to be 46 ± 3° (López-Martín et al. 2003). These values indicate that the large-scale disk is far from edge-on, which makes

it difficult to lift material in the outer disk into the line of sight. In fact, the hydrodynamical simulations of the tidal arm scenario by Dai et al. (2015) give a best fitting value of 64° for the inclination, and thus does not match the constraints from observations.

On the other hand, the modelling of K-band Keck interferometric observations tracing the continuum and gas in the inner region of the disk results in an inclination angle of 75° (Eisner et al. 2014, Table 6) for an emitting region within a fraction of 1 AU. This is a significantly higher inclination and closer to edge-on than for the outer disk. We note that some of the Keck interferometer data for RW Aur A was taken during the first eclipse in 2010/11. The discrepancy in the inclinations between inner and outer disk may be evidence for a large-scale warp in the disk, possibly caused by interaction with the companion RW Aur B. Thus, RW Aur B may have an effect on the disk, but it is unlikely to be the direct cause of the feature that eclipses RW Aur A.

Adopting the value from the inner disk for the disk inclination, the material in the occulting screen needs to be vertically displaced from the disk midplane by at least 0.26 times the distance from the central object. This value is comparable to the maximum vertical extent of the inner disk found in the so-called "dippers", T Tauri stars with periodic eclipses caused by disk warps caused by accretion channelled by a magnetic field tilted with respect to the rotational axis (Bouvier et al. 1999; McGinnis et al. 2015). RW Aur is not known to be a dipper, perhaps because the tilt of its magnetic field is not sufficient. Based on the high value for the inner disk inclination, however, it is conceivable that a magnetically driven disk wind can lift material into the line of sight.

The jet of RW Aur A has been extensively studied with high-resolution imaging. It is one of the densest among the T Tauri stars investigated in detail, but the mass outflow rate seems to be stable within an order of magnitude along the jet axis and in both lobes at 10^{-9} to $10^{-8}\,M_{\odot}\mathrm{yr}^{-1}$ (Melnikov et al. 2009). However, in the past there have been clear indications for strong variability in the forbidden lines caused by the wind as well as in the blue-shifted portion of Hα (Alencar et al. 2005).

In the standard scenario of magnetospheric accretion, the wind is thought to be coupled to the accretion, thus, we would expect that a change in the outflow rate or geometry, as indicated by our interpretation of the RW Aur dimming, is preceded by strong variability in the accretion flow. As far as we are aware, there is no evidence for a recent accretion burst in RW Aur. Its accretion rate is relatively high (10^{-7} to $10^{-6}\,M_{\odot}\mathrm{yr}^{-1}$) compared with other CTTS with similar mass, but seems to be relatively stable (e.g., Costigan et al. 2014). Thus, changes in the wind characteristics might not always be coupled to changes in the accretion properties. One possible trigger for a wind outburst could be an interaction between the disk and the putative stellar or substellar spectroscopic companion to RW Aur A (Gahm et al. 1999; Petrov et al. 2001). However, it is unclear how such an interaction can produce the sudden onset of wind activity multiple times over the course of the last ~ 7 years, with no precedents observed in the previous ~ 50 years. Another alternative may be that the fly-by of RW Aur B has caused an instability in the disk of RW Aur A, although modelling this scenario is beyond the scope of this study.

We encourage further multi-band photometric and spectroscopic monitoring of accretion and outflow signatures of RW Aur to further test and solidify our understanding of the system.

5 ACKNOWLEDGEMENTS

We acknowledge with thanks the variable star observations from the AAVSO International Database contributed by observers worldwide and used in this research. This publication also makes use of data products from NEOWISE, which is a project of the Jet Propulsion Laboratory/California Institute of Technology, funded by the Planetary Science Division of the National Aeronautics and Space Administration. The Liverpool Telescope is operated on the island of La Palma by Liverpool John Moores University in the Spanish Observatorio del Roque de los Muchachos of the Instituto de Astrofisica de Canarias with financial support from the UK Science and Technology Facilities Council. This work makes use of observations from the LCOGT network, taken under programs STA2014B-002 and STA2015A-002. The authors acknowledge support from the Science & Technology Facilities Council through grants no.ST/K502339/1 and ST/M001296/1 and the Science Foundation Ireland through grant no.10/RFP/AST2780.

REFERENCES

Alencar S. H. P., Basri G., Hartmann L., Calvet N., 2005, A&A, 440, 595
Antipin S., et al., 2015, Information Bulletin on Variable Stars, 6126, 1
Appenzeller I., Oestreicher R., Jankovics I., 1984, A&A, 141, 108
Barnsley R. M., Smith R. J., Steele I. A., 2012, Astronomische Nachrichten, 333, 101
Bouvier J., Covino E., Kovo O., Martin E. L., Matthews J. M., Terranegra L., Beck S. C., 1995, A&A, 299, 89
Bouvier J., et al., 1999, A&A, 349, 619
Brown T. M., et al., 2013, PASP, 125, 1031
Cabrit S., Pety J., Pesenti N., Dougados C., 2006, A&A, 452, 897
Cardelli J. A., Clayton G. C., Mathis J. S., 1989, ApJ, 345, 245
Cody A. M., et al., 2014, AJ, 147, 82
Costigan G., Vink J. S., Scholz A., Ray T., Testi L., 2014, MNRAS, 440, 3444
Dai F., Facchini S., Clarke C. J., Haworth T. J., 2015, MNRAS, 449, 1996
Eisner J. A., Hillenbrand L. A., Stone J. M., 2014, MNRAS, 443, 1916
Fukugita M., Ichikawa T., Gunn J. E., Doi M., Shimasaku K., Schneider D. P., 1996, AJ, 111, 1748
Gahm G. F., Petrov P. P., Duemmler R., Gameiro J. F., Lago M. T. V. T., 1999, A&A, 352, L95
Ghez A. M., Neugebauer G., Matthews K., 1993, AJ, 106, 2005
Ghez A. M., White R. J., Simon M., 1997, ApJ, 490, 353
Hartigan P., Edwards S., Ghandour L., 1995, ApJ, 452, 736
Herbst W., Herbst D. K., Grossman E. J., Weinstein D., 1994, AJ, 108, 1906
Joy A. H., 1945, ApJ, 102, 168
López-Martín L., Cabrit S., Dougados C., 2003, A&A, 405, L1
Mainzer A., et al., 2011, ApJ, 731, 53
Mainzer A., et al., 2014, ApJ, 792, 30
McGinnis P. T., et al., 2015, A&A, 577, A11
Melnikov S. Y., Eislöffel J., Bacciotti F., Woitas J., Ray T. P., 2009, A&A, 506, 763
Mohanty S., Jayawardhana R., Basri G., 2005, ApJ, 626, 498
Monet D. G., et al., 2003, AJ, 125, 984
Petrov P. P., Gahm G. F., Gameiro J. F., Duemmler R., Ilyin I. V., Laakkonen T., Lago M. T. V. T., Tuominen I., 2001, A&A, 369, 993
Petrov P. P., Gahm G. F., Djupvik A. A., Babina E. V., Artemenko S. A., Grankin K. N., 2015, A&A, 577, A73
Rodriguez J. E., Pepper J., Stassun K. G., Siverd R. J., Cargile P., Beatty T. G., Gaudi B. S., 2013, AJ, 146, 112
Rodriguez J. E., et al., 2016, AJ, 151, 29
Schneider P. C., et al., 2015, A&A, 584, L9
Scholz A., Xu X., Jayawardhana R., Wood K., Eislöffel J., Quinn C., 2009, MNRAS, 398, 873
Scholz A., Bozhinova I., Lux O., Pannicke A., Mugrauer M., 2016, The Astronomer's Telegram, 9428

Shenavrin V. I., Petrov P. P., Grankin K. N., 2015, Information Bulletin on Variable Stars, 6143, 1
Skinner S. L., Güdel M., 2014, ApJ, 788, 101
Steele I. A., et al., 2004, in Oschmann Jr. J. M., ed., Proc. SPIEVol. 5489, Ground-based Telescopes. pp 679–692, doi:10.1117/12.551456
Takami M., et al., 2016, ApJ, 820, 139
White R. J., Hillenbrand L. A., 2004, ApJ, 616, 998